# Quantitative surface structure determination using in situ high-energy SXRD: Surface oxide formation on Pd(100) during catalytic CO oxidation

CrossMark

Mikhail Shipilin [a,*], Uta Hejral [b,c], Edvin Lundgren [a], Lindsay R. Merte [a], Chu Zhang [a], Andreas Stierle [b,c], Uta Ruett [c], Olof Gutowski [c], Magnus Skoglundh [d], Per-Anders Carlsson [d], Johan Gustafson [a]

[a] Division of Synchrotron Radiation Research, Lund University, Lund, Sweden
[b] University of Hamburg, Hamburg, Germany
[c] Deutsches Elektronen-Synchrotron (DESY), Hamburg, Germany
[d] Competence Centre for Catalysis, Chalmers University of Technology, Göteborg, Sweden

### ABSTRACT

We have performed a quantitative structure determination of the $\left(\sqrt{5}\times\sqrt{5}\right)$R27° surface oxide, formed on Pd(100) under semi-realistic conditions for catalytic CO oxidation, using in situ high-energy surface X-ray diffraction. We describe the experiment and the extraction of quantitative data in detail. The structural results are in agreement with previous reports of a system consisting of a single layer of PdO(101) formed in pure $O_2$ on top of Pd(100) and studied under ultra-high vacuum conditions.

© 2014 The Authors. Published by Elsevier B.V. This is an open access article under the CC BY-NC-ND license (http://creativecommons.org/licenses/by-nc-nd/3.0/).

## 1. Introduction

The possibility to follow processes in situ on the atomic level is of great importance for numerous fields within science and technology. One prominent example is heterogeneous catalysis, where atomic processes on the surface of catalysts play a key-role and consequently have been studied intensively [1]. However, the atomic-scale surface structure during a catalytic reaction, under semi-realistic conditions, has been almost impossible to determine, due to the absence of a suitable experimental technique. Although surface structural determinations of model catalysts under highly active conditions have been attempted previously [2], a significant step forward in collecting quantitative data on a much improved timescale was reported recently [3].

Palladium is used in catalytic converters to oxidize CO and hydrocarbons [4]. Surprisingly, despite years of efforts, the active surface phase of the seemingly simple CO oxidation reaction over Pd single crystal surfaces, acting as model catalysts, is still under debate [5,6]. Part of the controversy lies in the differences between the techniques that have been applied, and part in the extremely fast reaction and the short surface residence times for the species actively participating in the process [7–9].

Recent studies have shown that the catalytic CO oxidation reaction is fast in the presence of surface oxides formed under semi-realistic reaction conditions over Pd, Rh, Pt and Ru [5,8,10–15]. For Pd(100) a similar surface oxide structure has been reported previously, formed under ultra-high vacuum (UHV) conditions using molecular oxygen, and several models have been discussed in the literature.

In 1982, Orent and Bader suggested that the oxide structure is formed by a single plane of PdO(001) on the Pd(100) surface (see Fig. 1a) [16], which was later confirmed by quantitative low-energy electron diffraction (LEED) studies [17,18]. These results were, however, revised by a combination of high-resolution core-level spectroscopy (HRCLS), scanning tunneling microscopy (STM) and density functional theory (DFT) calculations [19]. In this study, a layer of PdO(100) (Fig. 1b) was examined, but was shown not to correspond to the expected HRCLS, DFT or STM results. Instead a model was suggested consisting of a single PdO(101) plane, which is similar to the PdO(100) layer except that half of the oxygen atoms are removed from the surface to be placed just underneath the Pd layer (Fig. 1c) [19]. The model was later refined and improved by a combined STM, DFT and quantitative LEED study [20]. The PdO(101) surface is of significant interest because of its coordinatively unsaturated (CUS) Pd atoms [21], which provide sites potentially attractive for adsorption and catalytic reactions, similar to the $RuO_2$(110) surface [22].

The contradiction of models, as well as the importance of the CUS sites, motivated us to study the atomic structure of the surface oxide

---

* Corresponding author. Tel.: +46 46 222 04 69.
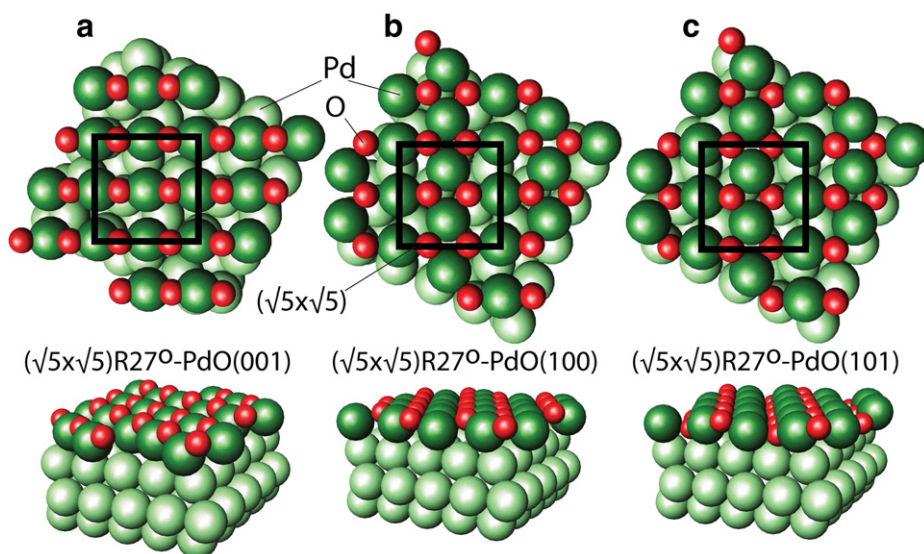*E-mail address:* mikhail.shipilin@sljus.lu.se (M. Shipilin).

**Fig. 1.** Ball-models of $Pd(100)-\left(\sqrt{5} \times \sqrt{5}\right)R27°-O$ structures considered in the present investigation: (a) PdO(001)/Pd(100), (b) PdO(100)/Pd(100), and (c) PdO(101)/Pd(100).

formed on the Pd(100) under highly active CO oxidation conditions. Further, while the surface exhibits the same periodicity $\left(\left(\sqrt{5} \times \sqrt{5}\right)R27°\right)$, the larger question is if the atomic-scale structure observed under UHV conditions [20] is the same as the structure present under semi-realistic reaction conditions [5,8]. Although attempts have been made previously to determine the atomic structure under reaction conditions using conventional surface X-ray diffraction (SXRD) [2], the collection of a full quantitative data set is in general too time-consuming to be performed in situ.

We recently demonstrated how high-energy (HE)SXRD, using 85 keV photons in combination with a two-dimensional detector, facilitates data acquisition such that the three-dimensional reciprocal surface lattice can be collected within a time frame reasonable for in situ studies during a catalytic steady state reaction [3]. The use of high-energy X-rays [23] for surface studies can be seen as an extension of conventional SXRD [24,25]. It allows obtaining the full structural information of the surface with a data quality that is suitable for quantitative analysis allowing determination of exact atomic positions.

In the present report, the diffraction geometry as well as the procedure of extraction and quantitative analysis of data obtained by HESXRD are described in detail. The procedure was applied to resolve the surface oxide structure formed on a Pd(100) single crystal when being highly catalytically active under semi-realistic conditions for the CO oxidation reaction. Our results confirm that the structure consists of a single layer of PdO(101) as found under UHV conditions. The results also indicate that, whereas SXRD is highly sensitive to the position of the Pd atoms, it is less sensitive to the exact position of the O atoms since they are weaker scatterers.

## 2. Experimental

The experiments were carried out at the beamline P07 of PETRA III at Deutsches Elektronen-Synchrotron (DESY) in Hamburg, Germany. This beamline is designed for materials studies with hard X-ray radiation and the energy of the beam is tunable between 30 and 200 keV. The beam itself can be focused on the sample to a spot of 3 μm by 40 μm [26]. In the present experiments we used 85 keV photons directed at the sample surface under an incident angle of 0.04°, close to the critical angle of total external reflection for Pd, to achieve high surface sensitivity.

To create the desired environment for catalytic reactions a specially designed UHV chamber/reactor was used [27]. It allows pressures in the

$10^{-10}$ mbar range for surface preparation as well as a controlled gas pressure up to 1 bar in the reactor chamber. The gas supply system allows independently setting the reactor pressure, gas composition and total gas flow. To follow the reaction process, i.e. changes of the gas composition in the reactor, a residual gas analyzer (RGA 200) from Stanford Research Systems was used.

The resulting diffraction patterns were collected with a 410 × 410 mm$^2$ Perkin-Elmer flat panel detector, consisting of CsI scintillators on amorphous silicon photodiodes, adapted for energies above 20 keV. The detector has the resolution of 4 Mpx with 200 × 200 μm$^2$ physical size of an individual pixel. To protect it from oversaturation due to highly intense Bragg reflections from the Pd substrate, parts of the detector were covered with Densimet® pieces. The presence of this protection causes black rectangular shapes in the detector images (see Fig. 2a–c). Further, to shield the detector from radiation scattered by the Be walls of the reactor, a specially designed mask made of tungsten was placed between the reactor and the detector, generating circular shadows in the bottom-center and top-corners of the images.

During the experiment the sample was continuously exposed to a photon flux in the order of $5 \times 10^{10}$ photons/s. The diffraction pattern did not show any changes with the time of exposure indicating that there were no continuous effects connected to beam damage.

Before the measurements the sample was cleaned by cycles of Ar$^+$ sputtering and annealing at 1000 K until the diffraction pattern indicated a clean Pd(100) surface. The surface oxide structure was formed and investigated in a flow of about 2 ml$_n$/min O$_2$ (1 ml$_n$ is the amount of gas corresponding to 1 ml at standard pressure and temperature), 4 ml$_n$/min CO and 25 ml$_n$/min Ar, i.e. close to the stoichiometric ratio between CO and O$_2$ for complete oxidation to CO$_2$, at a sample temperature of 600 K. The total pressure in the reactor was 100 mbar. Under these conditions the sample was highly catalytically active, converting all CO reaching the surface to CO$_2$.

The tetragonal basis set of vectors $\mathbf{a}_1$, $\mathbf{a}_2$ lying in the surface plane and $\mathbf{a}_3$ perpendicular to them was used to describe the crystal structure. In terms of the bulk lattice constant $a_0$ ($a_0(Pd) = 3.89$ Å) the lengths of these vectors can be expressed as $|\mathbf{a}_1| = |\mathbf{a}_2| = a_0/\sqrt{2}$ and $|\mathbf{a}_3| = a_0$.

## 3. Data collection and treatment

Due to the high energy of the X-rays and the large size of the 2D detector mounted at a distance of 1800 mm from the sample, the part of reciprocal space from $-5$ Å$^{-1}$ to 5 Å$^{-1}$ and from 0 Å$^{-1}$ to 5 Å$^{-1}$ in
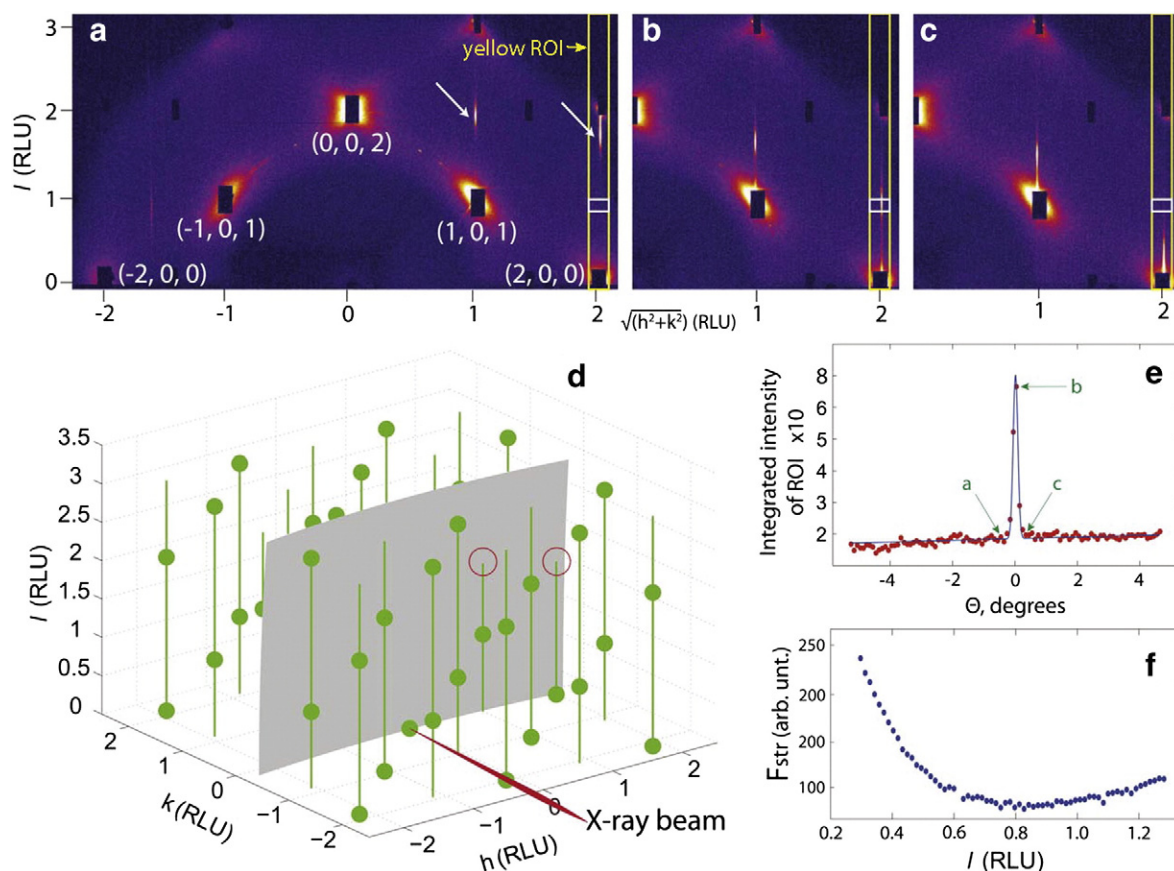
**Fig. 2.** (a–c) Images 49, 54 and 57 of a 100-images data set revealing the sequential appearance of a CTR at $h = 2$ RLU and $k = 0$ RLU at $-0.5$, 0 and 0.3° within the interval from $-5.3$ to 4.6° of the sample azimuthal rotation relatively to h-axis in reciprocal space (for panels (b–c) non-informative parts are not included). The yellow rectangle labeled as "yellow ROI" in panel (a) shows the detector area chosen for the rod data extraction, the small white rectangle shows one of the ROIs along the rod within the yellow rectangle. The white arrows indicate where the CTRs intersect with the Ewald sphere, the same regions are marked with red circles in panel (d). (d) 3D-model of reciprocal space containing Bragg reflections and diffraction rods from the clean Pd(100) surface (gray shape represents detectable area, the part of the Ewald sphere intersecting with the rods). (e) The intensity integrated over the white rectangle in panels (a–c) versus azimuthal angle of the sample rotation (the values corresponding to images (a–c) are marked with green arrows). (f) The final values of structure factor along the rod. Note that only the part between $l = 0.3$ RLU and $l = 1.3$ RLU is considered for processing since shadows from Densimet® protection pieces and tungsten mask affect the experimental intensity at other $l$ values for this rod. The same procedure is applied to all other rods.

in-plane and out-of-plane directions, respectively, can be probed simultaneously corresponding to a slice in reciprocal space at a fixed sample azimuth. In the case of Pd(100) this part contains diffraction peaks with $h$ and $k$ values up to 2 and an $l$ value up to 3 reciprocal lattice units (RLU). Fig. 2a shows the diffraction from Pd(100) corresponding to the orientation of the Ewald sphere and the crystal reciprocal lattice as shown in panel Fig. 2d. Two crystal truncation rods (CTRs) intersect the Ewald sphere (marked with circles in Fig. 2d) and consequently appear in the detector image (marked with white arrows in panel Fig. 2a). In addition, a superstructure rod is present on the left side of the detector image in panel Fig. 2a, which is not included in the map in Fig. 2d.

In the ideal situation, the CTRs as well as the Ewald sphere would have been infinitely thin and the intersection point would be a sharp spot. In reality, however, there is a certain degree of mosaicity in the sample, which gives rise to an elongation of the diffraction spots in the $l$ direction. Fig. 3 shows a schematic slice of the Ewald sphere and the scattering vector $\mathbf{q} = \mathbf{k}_f - \mathbf{k}_i$ at a fixed rotational angle $\theta$. The single crystal shown at the bottom is not perfect but consists of small domains of size $D$. Apart from perfectly aligned domains (represented by orange cubes) there are others that are tilted around the surface normal (blue and green cubes). Due to the tilted domains, a rod is also probed above (blue domains) and below (green domains) the expected $l$ value, even at a fixed rotational angle $\theta$. In addition, due to the same surface mosaicity, the distribution of the signal, obtained at a specific $l$ value by

a rotation of the sample in $\Delta\theta$ range around the current rotational position, has a Gaussian-like shape shown as an inset in Fig. 3 with a FWHM of $\Delta\theta$. In addition to the mosaicity, the finite domain size, $D$, leads to an enlargement of the intersection points by $\Delta\mathbf{q}_D$, and the energy distribution $\Delta E$ of the X-ray beam results in a certain thickness, $\Delta k_i$ of the Ewald sphere. All above mentioned corrections are explained in detail in ref. [25] for the case of a point-detector. With the wide angular acceptance of the large 2D detector we do not need to consider all of them for the analysis of the present data. The applied correction factors will be described below.

The 3D reciprocal lattice is collected through a simple rotation of the sample around the surface normal while continuously recording detector images, in the present case every 0.1° clockwise. This results in the intersection area between the CTRs and the Ewald sphere to move along the $l$ direction as seen in Fig. 2a–c showing three snapshots during such a rotation with 0.5° and 0.3° angular intervals between a and b and between b and c respectively.

In order to extract data for quantitative analysis, we have written a plugin for ImageJ (Image processing and analysis software) [28] using the Java Development Environment. The process of data extraction and treatment has recently been discussed in detail in the case of a smaller non-stationary 2D-detector and lower X-ray energies in [29]. In the present case, the extraction process is technically different and is illustrated in Fig. 2. First, the sequence of images (100 images in this case), where the rod of interest (CTR at $h = 2$ RLU and $k = 0$ RLU)
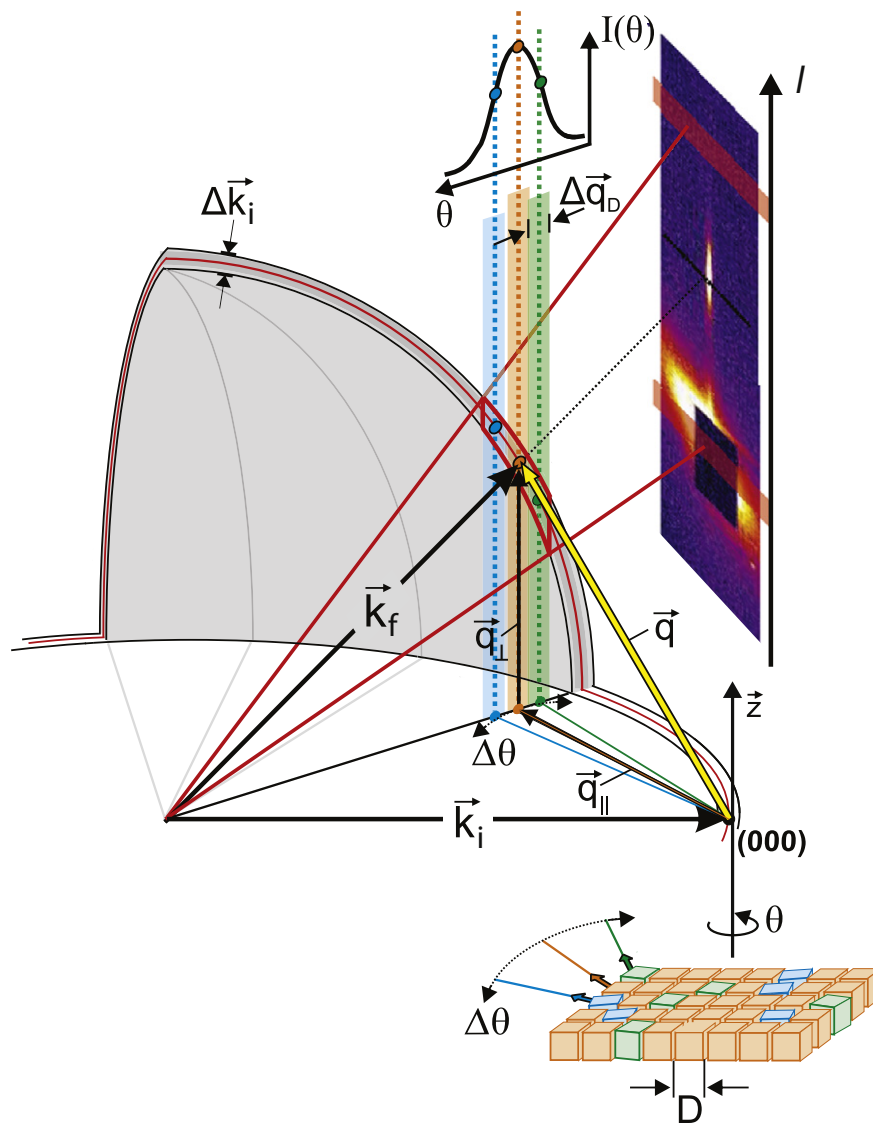
**Fig. 3.** Sketch of the Ewald sphere and the resulting diffraction pattern recorded at a fixed rotational angle θ for the non-ideal sample surface with mosaicity. The energy distribution of the incoming beam, as well as the mutual misalignment and finite size of the mosaicity domains, leads to an elongation of the intersection of the diffraction rod with the Ewald sphere and therefore to an elongation of the detected signal.

appears was identified. Second, a region of interest containing this rod (yellow rectangle labeled as "yellow ROI" in Fig. 2a–c) was defined and divided into smaller equal parts (such as the white rectangle in Fig. 2a–c). The integrated intensity of each smaller region, as a function of rotational angle, was extracted as shown in Fig. 2e. Third, a Gaussian function with a linear background was fitted to this data to obtain the integrated intensity of the diffraction rod at the current $l$ value.

The resulting values of intensity along the rod can be converted to the corresponding structure factors, $F_{str}$, according to $I_{int} = p \cdot |F_{str}|^2 \cdot C_{tot}$, where $p$ is the constant considering properties of the sample and the incident beam and $C_{tot}$ is the total correction factor taking into account the characteristic features of the experiment geometry [30,31]. Because of the experimental conditions in the present set-up, the corrections are significantly simplified. High linear horizontal polarization of the incident beam allows excluding the vertical polarization correction factor from the calculations. The wide angular range of the sample rotation eliminates the correction factor for in-plane detector acceptance since the in-plane momentum transfer component of the signal is collected. Because of the micrometer-sized beam, the open-slit geometry and the large 2D detector, the beam area and the beam profile correction factors are excluded.

In summary, the total correction factor used for calculations in the present case can be represented as $C_{tot} = C_{hp} \cdot C_L \cdot C_{rod} \cdot C_d \cdot C_i$, where $C_{hp}$ is a horizontal polarization correction factor, $C_L$ — Lorentz correction factor, $C_{rod}$ — rod interception correction factor, $C_d$ — solid scattering angle correction factor, and $C_i$ — beam inclination correction factor [3].

The last two correction factors are induced by difference in detector pixel positions relatively to the scattered beam, i.e. different distance from the sample and non-normal incidence of the scattered beam. The angular values required for the calculations of the applied corrections were either already known from the corresponding motor positions or calculated using the distance from the sample to the detector, and from the size of the detector and the pixels.

The calculated structure factors can be plotted versus the corresponding $l$ values, as shown in Fig. 2f, revealing the shape of the CTR, which contains information about the surface structure on the atomic scale. Error bars were estimated to be within 10% by comparing symmetry-equivalent diffraction rods. For the quantitative analysis, model based structure factor values are calculated, compared and fitted to the experimental values using the ANA-ROD software package [32].

## 4. Results and discussion

In a close to stoichiometric mixture of CO and $O_2$ at a sample temperature of 600 K, a surface oxide structure with a $\left(\sqrt{5} \times \sqrt{5}\right)R27°$ surface periodicity was found on Pd(100), while simultaneous mass spectrometry revealed high catalytic activity for CO oxidation into $CO_2$. A similar surface oxide structure with the same $\left(\sqrt{5} \times \sqrt{5}\right)R27°$ periodicity has been reported previously, both under reaction conditions and in pure oxygen, and several models have been suggested [16–20].

Fig. 4a shows a qualitative representation of the HESXRD data, where 900 detector images acquired during a 90° rotation of the sample are combined into one image in such a way that each pixel contains the highest intensity value for this particular pixel position over the entire data sequence. In such an image, the rotational information is lost, but it allows us to observe and identify the different CTRs as well as the superstructure rods.

To extract the reciprocal space coordinates of the rods, each pixel in the detector was recalculated from lab coordinates to reciprocal lattice units according to the geometry of the experimental setup and the curvature of the Ewald sphere. As a result a 3D map of the reciprocal space for the system (Fig. 4b–d), as well as a hk-map at any accessible L-value (Fig. 4e for $l = 0.5$ RLU), can be obtained. The latter data representation results in an image which resembles a LEED pattern displaying the in-plane positions (h-, k-coordinates) of each diffraction rod. As the LEED pattern, this in-plane image can be used to determine the surface periodicity, which in this case is close to a $\left(\sqrt{5} \times \sqrt{5}\right)R27°$ as expected.

The high resolution in the current measurements exceeds that of conventional LEED and allows observing the mismatch between the $Pd(100) - \left(\sqrt{5} \times \sqrt{5}\right)R27° - O$ surface structure and the structure of the underlying Pd(100) [20], which will be elucidated in more detail in a separate publication. In the present paper, the sum of intensities in the vicinity of the diffraction rod is used for the quantitative analysis. The values of the structure factor for 8 CTRs and 23 superstructure rods accessible within 90° sample rotation were extracted and compared to those calculated using the ANA-ROD software package. Due to the four-fold symmetry of the system some of these rods are symmetry equivalent resulting in a total of 9 in-equivalent rods used for the structure determination.

As described above, three different models, corresponding to a single layer of PdO(001), PdO(100) and PdO(101), have been used in the analysis. For the present measurements, inclusion of two PdO layers to the model gave rise to a worse agreement between the calculated and measured data. In case of an epitaxial multilayer PdO film, bulk Bragg reflections in the diffraction pattern should be observed, which clearly is not the case for the present data. Thus, our data strongly suggest that under the present conditions, we have a single PdO layer present on the surface. For PdO(001) and PdO(101) we have used the atomic
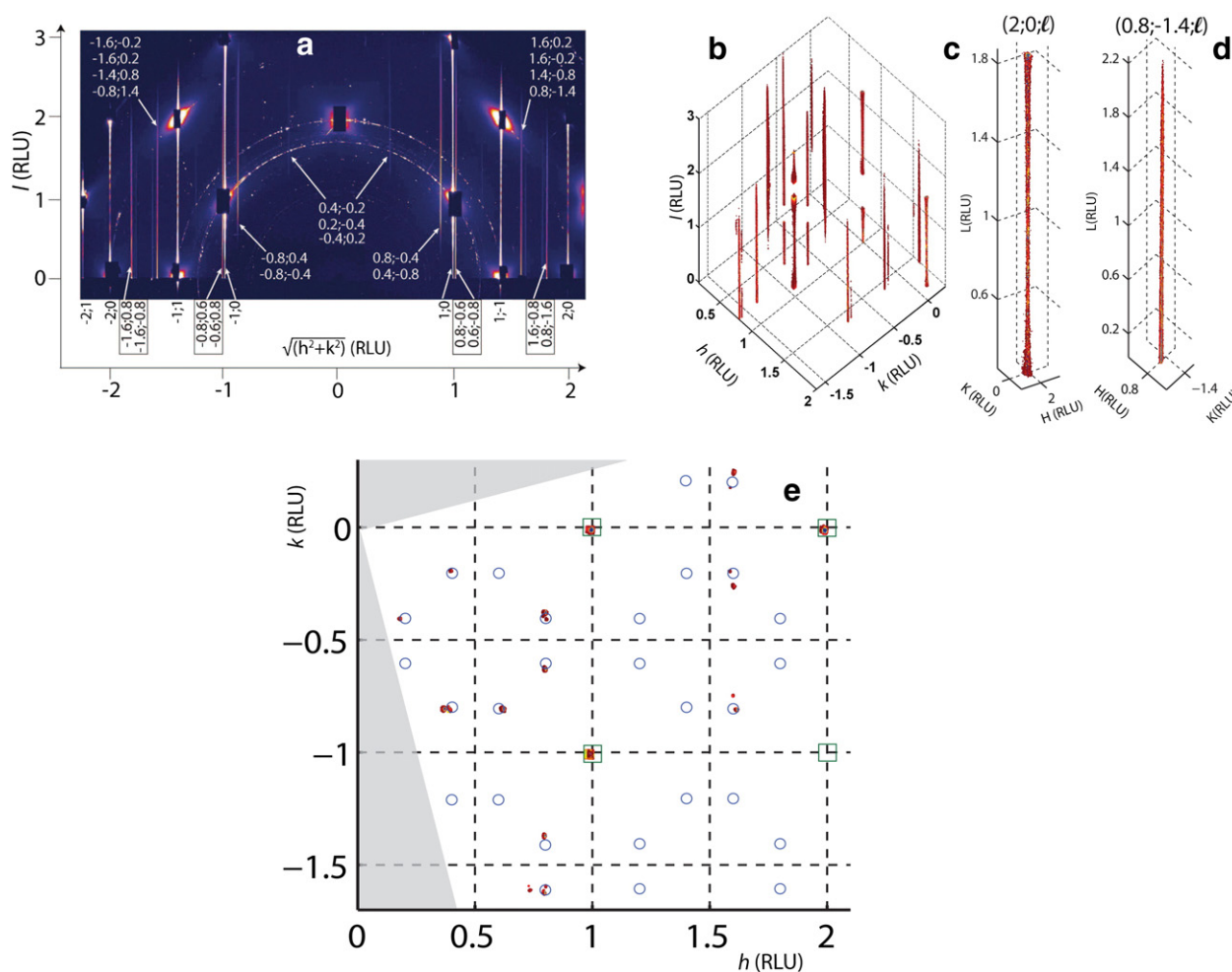


**Fig. 4.** (a) Image with each pixel containing the highest intensity for this particular pixel position over 900 images obtained for a 90° rotation of the Pd(100) single crystal under CO oxidation reaction conditions (2 ml$_n$/min $O_2$ (1 ml$_n$ is the amount of gas corresponding to 1 ml at standard pressure and temperature), 4 ml$_n$/min CO and 25 ml$_n$/min Ar, 100 mbar total pressure in the reactor and a sample temperature of 600 K). h, k-values for the observed rods in the image are marked. (b) Part of a 3D reciprocal map of the system restored from image sequence. (c–d) 3D shapes of individual diffraction rods. (e) Part of h, k-map of reciprocal space at $l = 0.5$ RLU for the same system (borders of the space probed via 90° sample rotation are marked, green rectangles and blue circles mark the expected positions of CTRs and superstructure rods correspondingly for the case of $\left(\sqrt{5} \times \sqrt{5}\right)R27°$ perfectly matching the substrate).
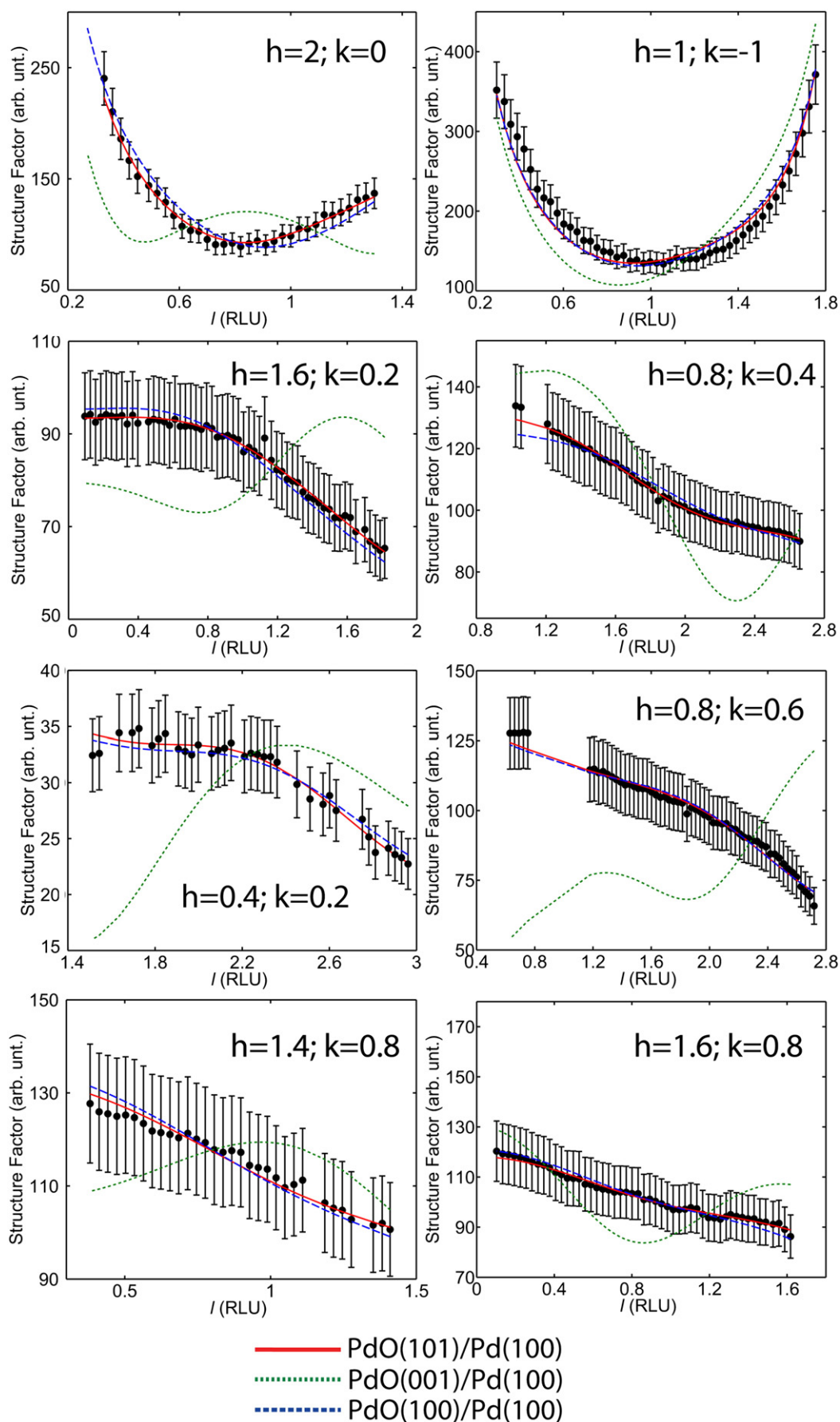
**Fig. 5.** Experimental (black dots) and calculated (green dotted line for PdO(001), blue dashed line for PdO(100) and red solid line for PdO(101)) values of the structure factor for symmetrically non-equivalent CTRs and superlattice rods.

coordinates reported by Saidy et al. [18] and Kostelnik et al. [20], respectively, without any changes. To investigate the agreement between our data and those for a PdO(100) layer, we have used the atomic coordinates of the PdO(101), as reported by Kostelnik et al., but moved the subsurface oxygen layer to the surface. For each model, 8 structural domains were considered (4 domains of the structure rotated by 90° relative to each other and the 4 corresponding mirrored domains).

The results of the quantitative analysis are summarized in Fig. 5, where the black experimental data points are compared to the best fits of the PdO(001) (green dotted line), PdO(100) (blue dashed line) and PdO(101) (red solid line) models. It is obvious that the PdO(001) model does not fit, while both the PdO(100) and PdO(101) orientations reproduce the experimental data well. At first glance this observation might appear surprising, however, it can be explained by the difference in scattering strength between Pd and O. The quasi-hexagonal Pd lattice is the same in both structures, and, since x-ray scattering factor scales with $Z^2$ ($Z^2 = 2116$ for Pd and 64 for O), the contribution from the O atoms is relatively weak. In order to distinguish between the two models, one instead has to turn to other methods such as high-pressure X-ray photoelectron spectroscopy (HPXPS), which shows that there are two different oxygen layers in the surface oxide structure both under UHV [19] and semi-realistic reaction conditions [9], hence disqualifying the PdO(100) model.

## 5. Summary

We describe how HESXRD experiments are performed and analyzed to resolve the atomic structure of the $\left(\sqrt{5} \times \sqrt{5}\right)R27°$ surface oxide formed on Pd(100) under semi-realistic CO oxidation conditions. The scattering geometry, the appearance of scattered intensity on the detector as well as the details of the data extraction are described. We find that the use of high-energy X-rays facilitates the data collection, the alignment procedure, the interpretation of SXRD as well as the application of correction factors. Once a proper data treatment procedure is available as a software, the data extraction is also facile. In general, HESXRD is a step forward for surface structure determinations, in particular under harsh conditions, limited only by the number of suitable beamlines.

An important point is that HESXRD enables quantitative structure determinations to be performed within a time-frame suitable for in situ studies.

The present results show that the model consisting of a single PdO(001) layer does not fit the experimental data, while both PdO(101) and PdO(100) matches the data well. The large difference in scattering factor (which scales with $Z^2$) between Pd and O makes (HE)SXRD rather insensitive in the present case to the position of the O atoms demanding complementary experimental and theoretical studies to distinguish between the two structures. Finally it is possible to conclude that the present structure consists of single layer of PdO(101).

## References

[1] G. Ertl, H. Knözinger, J. Weitkamp, Handbook of Heterogeneous Catalysis, Wiley-VCH, Weinheim, 2008.
[2] R. Westerström, J.G. Wang, M. Ackermann, J. Gustafson, A. Resta, A. Mikkelsen, J.N. Andersen, E. Lundgren, O. Balmes, X. Torrelles, J.W.M. Frenken, B. Hammer, J. Phys. Condens. Matter 20 (2008) 184019.
[3] J. Gustafson, M. Shipilin, C. Zhang, A. Stierle, U. Hejral, U. Ruett, O. Gutowski, P.-A. Carlsson, M. Skoglundh, E. Lundgren, Science 343 (2014) 758.
[4] J. Kašpar, P. Fornasiero, N. Hickey, Catal. Today 77 (2003) 419.
[5] R. Van Rijn, O. Balmes, R. Felici, J. Gustafson, D. Wermeille, R. Westerström, E. Lundgren, J.W.M. Frenken, J. Phys. Chem. C 114 (2010) 6875.
[6] F. Gao, Y. Wang, D.W. Goodman, J. Phys. Chem. C 114 (2010) 6874.
[7] F. Gao, Y. Wang, Y. Cai, D.W. Goodman, J. Phys. Chem. C 113 (2009) 174.
[8] R. Van Rijn, O. Balmes, A. Resta, D. Wermeille, R. Westerström, J. Gustafson, R. Felici, E. Lundgren, J.W.M. Frenken, Phys. Chem. Chem. Phys. 13 (2011) 13167.
[9] S. Blomberg, M.J. Hoffmann, J. Gustafson, N.M. Martin, V.R. Fernandes, A. Borg, Z. Liu, R. Chang, S. Matera, K. Reuter, E. Lundgren, Phys. Rev. Lett. 110 (2013) 117601.
[10] J. Gustafson, R. Westerström, A. Mikkelsen, X. Torrelles, O. Balmes, N. Bovet, J.N. Andersen, C.J. Baddeley, E. Lundgren, Phys. Rev. B 78 (2008) 045423.
[11] J. Gustafson, R. Westerström, A. Resta, A. Mikkelsen, J.N. Andersen, O. Balmes, X. Torrelles, M. Schmid, P. Varga, B. Hammer, G. Kresse, C.J. Baddeley, E. Lundgren, Catal. Today 145 (2009) 227.
[12] J. Gustafson, R. Westerström, O. Balmes, A. Resta, R. van Rijn, X. Torrelles, C.T. Herbschleb, J.W.M. Frenken, E. Lundgren, J. Phys. Chem. C 114 (2010) 4580.
[13] J. Gustafson, R. Westerström, O. Balmes, A. Resta, X. van Rijn, R. Torrelles, C.T. Herbschleb, J.W.M. Frenken, E. Lundgren, J. Phys. Chem. C 114 (2010) 22372.
[14] M.D. Ackermann, T.M. Pedersen, B.L.M. Hendriksen, O. Robach, S.C. Bobaru, I. Popa, C. Quiros, H. Kim, B. Hammer, S. Ferrer, J.W.M. Frenken, Phys. Rev. Lett. 95 (2005) 255505.
[15] H. Over, O. Balmes, E. Lundgren, Catal. Today 145 (2009) 236.
[16] T.W. Orent, S.D. Bader, Surf. Sci. 115 (1982) 323.
[17] D.T. Vu, K.A.R. Mitchell, O.L. Warren, P.A. Thiel, Surf. Sci. 318 (1994) 129.
[18] M. Saidy, O.L. Warren, P.A. Thiel, K.A.R. Mitchell, Surf. Sci. 494 (2001) L799.
[19] M. Todorova, E. Lundgren, V. Blum, A. Mikkelsen, S. Gray, J. Gustafson, M. Borg, J. Rogal, K. Reuter, J.N. Andersen, M. Scheffler, Surf. Sci. 541 (2003) 101.
[20] P. Kostelnik, N. Seriani, G. Kresse, A. Mikkelsen, E. Lundgren, V. Blum, T. Sikola, P. Varga, M. Schmid, Surf. Sci. 601 (2007) 1574.
[21] J.F. Weaver, Chem. Rev. 113 (2013) 4164.
[22] H. Over, Chem. Rev. 112 (2012) 3356.
[23] H. Reichert, V. Honkimäki, A. Snigirev, S. Engemann, H. Dosch, Phys. B Condens. Matter 336 (2003) 46.
[24] I.K. Robinson, Phys. Rev. Lett. 50 (1983) 1145.
[25] R. Feidenhans'l, Surf. Sci. Rep. 105 (1989).
[26] [online] http://photon-science.desy.de/facilities/petra_iii/beamlines/p07_high_energy_materials_science/index_eng.html .
[27] R. van Rijn, M.D. Ackermann, O. Balmes, T. Dufrane, A. Geluk, H. Gonzalez, H. Isern, E. de Kuyper, L. Petit, V.A. Sole, D. Wermeille, R. Felici, J.W.M. Frenken, Rev. Sci. Instrum. 81 (2010) 014101.
[28] [online] http://rsbweb.nih.gov/ij/.
[29] J. Drnec, T. Zhou, S. Pintea, W. Onderwaater, E. Vlieg, G. Renaud, R. Felici, J. Appl. Crystallogr. 47 (2014) 365.
[30] E. Vlieg, J. Appl. Crystallogr. 30 (1997) 532.
[31] C.M. Schlepütz, S.O. Mariager, S.A. Pauli, R. Feidenhans'l, P.R. Willmott, J. Appl. Crystallogr. 44 (2011) 73.
[32] [online] http://www.esrf.eu/computing/scientific/joint-projects/ANA-ROD/.